Inorganic Chemistry

Article

pubs.acs.org/IC

Pb(II)-Promoted Amide Cleavage: Mechanistic Comparison to a Zn(II) Analogue

Eric S. Elton,[†] Tingting Zhang,[‡] Rajeev Prabhakar,[‡] Atta M. Arif,[§] and Lisa M. Berreau*[,†]

[†]Department of Chemistry and Biochemistry, Utah State University, 0300 Old Main Hill, Logan, Utah 84322-0300, United States

[‡]Department of Chemistry, University of Miami, 1301 Memorial Drive, Coral Gables, Florida 33146-0431, United States

[§]Department of Chemistry, University of Utah, 315 S. 1400 E., Salt Lake City, Utah 84112-0850, United States

Supporting Information

ABSTRACT: Two new Pb(II) complexes of the amide-appended nitrogen/sulfur epppa (*N*-((2-ethylthio)ethyl)-*N*-((6-pivaloylamido-2-pyridyl)methyl)-*N*-((2-pyridyl)methyl)-amine) chelate ligand, [(epppa)Pb(NO_3)$_2$] (**4-NO_3**) and [(epppa)Pb(ClO_4)$_2$] (**4-ClO_4**), were prepared and characterized. In the solid state, **4-NO_3** exhibits κ^5-epppa chelate ligand coordination as well as the coordination of two bidentate nitrate ions. In acetonitrile, **4-NO_3** is a 1:1 electrolyte with a coordinated NO_3^-, whereas **4-ClO_4** is a 1:2 electrolyte. Treatment of **4-ClO_4** with 1 equiv $Me_4NOH{\cdot}5H_2O$ in CH_3CN:CH_3OH (3:5) results in amide methanolysis in a reaction that is akin to that previously reported for the Zn(II) analogue [(epppa)Zn](ClO_4)$_2$ (**3-ClO_4**). ^{1}H NMR kinetic studies of the amide methanolysis reactions of **4-ClO_4** and **3-ClO_4** as a function of temperature revealed free energies of activation of 21.3 and 24.5 kcal/mol, respectively. The amide methanolysis reactions of **4-ClO_4** and **3-ClO_4** differ in terms of the effect of the concentration of methanol (saturation kinetics for **4-ClO_4**; second-order behavior for **3-ClO_4**), the observation of a small solvent kinetic isotope effect (SKIE) only for the reaction of the Zn(II)-containing **3-ClO_4**, and the properties of an initial intermediate isolated from each reaction upon treatment with $Me_4NOH{\cdot}5H_2O$. These experimental results, combined with computational studies of the amide methanolysis reaction pathways of **4-ClO_4** and **3-ClO_4**, indicate that the Zn(II)-containing **3-ClO_4** initially undergoes amide deprotonation upon treatment with $Me_4NOH{\cdot}5H_2O$. Subsequent amide protonation from coordinated methanol yields a structure containing a coordinated neutral amide and methoxide anion from which amide cleavage can then proceed. The rate-determining step in this pathway is either amide protonation or protonation of the leaving group. The Pb(II)-containing **4-ClO_4** instead directly forms a neutral amide-containing, epppa-ligated Pb(II)−OH/Pb(II)-OCH_3 equilibrium mixture upon treatment with $Me_4NOH{\cdot}5H_2O$ in methanol. The rate-determining step in the amide methanolysis pathway of **4-ClO_4** is nucleophilic attack of the Pb(II)-OCH_3 moiety on the coordinated amide. Overall, it is the larger size of the Pb(II) center and the availability of coordination positions that enable direct formation of a Pb(II)−OH/Pb(II)-OCH_3 mixture versus the initial amide deprotonation identified in the reaction of the Zn(II)-containing **3-ClO_4**.

INTRODUCTION

Lead is a toxic environmental pollutant that has dramatic effects in biological systems even in small amounts. Even after the elimination of leaded gasoline, lead poisoning continues to be a problem in the United States, with about 5% of children being affected.[1] While the exact process by which lead poisoning occurs is not completely defined, it is known that lead binds to sulfur rich sites in proteins, often displacing Zn(II).[2] Recent small molecule and peptide studies have focused on examining the coordination chemistry of Pb(II) in Zn(II)-binding environments.[3−11] However, these studies do not include comparisons of biologically relevant reactivity, which might provide additional insight into the toxic properties of Pb(II).

Studies of zinc-promoted amide cleavage reactions continue to be an active area of research. This is due to the important role that mononuclear zinc centers play in catalyzing amide cleavage reactions that are directly involved in human health and disease,[12−14] as well as in reagents for the selective cleavage of peptides.[15−17] Despite the importance of zinc-promoted amide cleavage reactions, few detailed investigations of the kinetics and thermodynamics of such reactions involving a nonactivated amide substrate have been reported.[18−20] A strategy typically utilized in such systems has been the attachment of the amide to a chelate ligand so as to position the metal ion close to the scissile bond, such as in **1**−**3** (Scheme 1). In our laboratory, we have previously investigated the amide methanolysis or hydrolysis reactions of **2** and **3-ClO_4**.[19,21−23]

The interactions of Pb(II) with amide-containing ligands has been previously investigated.[2,24−26] However, to our knowledge, no examples of Pb(II)-promoted hydrolysis or alcoholysis of an amide linkage have been previously reported. In the studies outlined herein, we have examined amide cleavage reactivity in a system wherein the Zn(II) center can be replaced by Pb(II). Using as a starting point our previously reported

Received: July 10, 2013
Published: September 25, 2013

dx.doi.org/10.1021/ic401782x | *Inorg. Chem.* 2013, 52, 11480−11492

Scheme 1

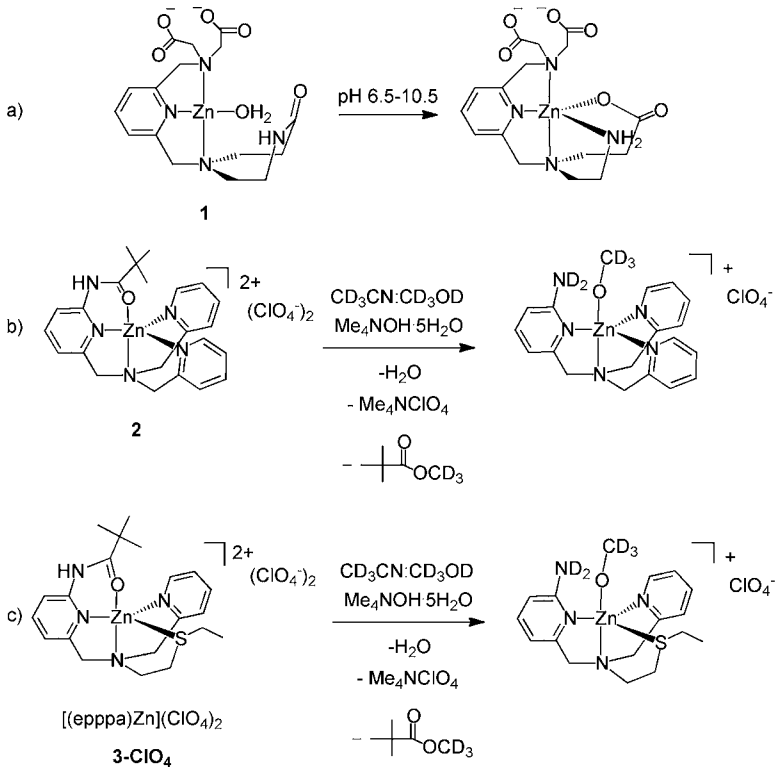

amide cleavage studies of $[(epppa)Zn](ClO_4)_2$ (**3-ClO$_4$**, epppa = *N*-((2-ethylthio)ethyl)-*N*-((6-pivaloylamido-2-pyridyl)-methyl)-*N*-((2-pyridyl)methyl)amine; Scheme 1),[22] we first prepared and fully characterized two new Pb(II) complexes, $[(epppa)Pb(ClO_4)_2]$ (**4-ClO$_4$**) and $[(epppa)Pb(NO_3)_2]$ (**4-NO$_3$**), of the same chelate ligand. We then examined the kinetics and thermodynamics of the amide methanolysis reaction of **4-ClO$_4$** and compared the results to those obtained for **3-ClO$_4$**. Combined with investigations into the intermediates in the amide methanolysis reaction pathways, as well as computational studies of the amide methanolysis reaction pathway as a function of metal ion,[27,28] the research presented herein provides the first detailed insight into the influence of Pb(II) versus Zn(II) in a biologically relevant reaction. The results of this study reveal how the inherent chemical properties of Pb(II) influence an amide cleavage reaction.

EXPERIMENTAL SECTION

General Methods. All reagents were purchased from commercial sources and used as received unless otherwise noted. The chelate ligand *N*-((2-ethylthio)ethyl)-*N*-((6-pivaloylamido-2-pyridyl)methyl)-*N*-((2-pyridyl)methyl)amine (epppa) and the zinc complex $[(epppa)Zn](ClO_4)_2$ (**3-ClO$_4$**) were prepared as previously described.[22]

Physical Methods. All NMR spectra for compound characterization were obtained on either a JEOL ECX-300 or Bruker ARX400 spectrometer at ambient temperature. Spectra are referenced to the residual solvent peak(s) in CHD_2CN (^{1}H 1.94 ppm (quintet), $^{13}C\{^1H\}$ 1.39 ppm (heptet)). FTIR spectra were obtained on a Shimadzu FTIR-8400 as KBr pellets. Conductance measurements were made at 22(1) °C using a YSI model 31A conductivity bridge with a cell having a cell constant of 1.0 cm^{-1} and using Me_4NClO_4 as a 1:1 electrolyte standard, and $[(bnpapa)Ni](ClO_4)_2$[29] as a 1:2 standard. Solutions for conductance measurements were prepared as previously described.[30] Mass spectroscopy experiments for compound characterization were performed at the University of California, Riverside. Elemental analyses were performed by Atlantic Microlabs of Norcross, GA, using a PE2400 automatic analyzer.

Caution! *Perchlorate salts of metal complexes with organic ligands are potentially explosive. Only small amounts of material should be prepared, and these should be handled with great care.*[31]

*[(epppa)Pb(ClO$_4$)$_2$] (**4-ClO$_4$**).* To a solution of $Pb(ClO_4)_2{\cdot}3H_2O$ (54 mg, 0.11 mmol) in methanol (~2 mL) was added a solution of epppa (46 mg, 0.11 mmol) in methanol (~1 mL). The resulting mixture was stirred at ambient temperature for ~20 min after which time excess Et_2O (~15 mL) was added to induce precipitation of the product. After being allowed to settle overnight at −20 °C, the excess solvent was decanted and the deposited solid was dried under vacuum (91%). ^{1}H NMR (CD_3CN, 300 MHz) δ 9.06 (br, 1H, N-*H*), 8.92 (m, J = 5.4 Hz, 1H, α-H (py)), 8.08−7.98 (m, 2H, β-H (Py), γ-H (AmPy)), 7.68−7.62 (m, 2H, β-H (Py), γ-H (py)), 7.44 (d, J = 7.6 Hz, 1H, β-H (AmPy)), 7.37 (d, J = 8.2 Hz, 1H, β-H (AmPy)), 4.71 (d, J = 15.0 Hz, 1H, benzylic), 4.69 (d, J = 15.0 Hz, 1H, benzylic), 4.52 (d, J = 15.0 Hz, 1H, benzylic), 4.34 (d, J = 15.0 Hz, 1H, benzylic), 3.69−3.58 (m, 2H, CH_2 (ethylene linker)), 2.99−2.90 (m, 1H, CH (ethylene linker)), 2.64−2.52 (m, 3H, CH (ethylene linker) and CH_2 (ethyl)), 1.35 (s, 9H, $C(CH_3)_3$), 1.21 (t, J = 7.4 Hz, 3H, $-CH_3$ (ethyl)); $^{13}C\{^1H\}$ (CD_3CN, 100 MHz) δ 182.4, 159.8, 154.9, 151.8, 149.6, 143.3, 141.8, 126.0, 125.4, 122.6, 117.3, 62.6, 62.5, 60.3, 41.4, 29.3, 27.2, 26.7, 14.5 (19 resonances expected and observed); FTIR (KBr, cm^{-1}) 3397 (br, ν_{N-H}), 1656 ($\nu_{C=O}$), 1609, 1523, 1456, 1417, 1366, 1163 (ν_{ClO4}), 1096 (ν_{ClO4}), 1018 (ν_{ClO4}), 918 (ν_{ClO4}), 622 (ν_{ClO4}). Anal. Calcd for $C_{21}H_{30}Cl_2N_4O_9PbS$: C, 31.82; H, 3.81; N, 7.07. Found: C, 32.03; H, 3.89; N, 6.75.

*[(epppa)Pb(NO$_3$)$_2$] (**4-NO$_3$**).* This compound was prepared using $Pb(NO_3)_2$ in a synthetic route analogous to that used for **4-ClO$_4$** except with longer stirring time (~40 min). Precipitation of the product by Et_2O addition resulted in the deposition of a white powder (83%). Recrystallization of this powder by diethyl ether diffusion into a ^{i}PrOH:CH_3OH (1:1) solution yielded colorless crystals suitable for single crystal X-ray diffraction analysis. ^{1}H NMR (CD_3CN, 300 MHz) δ 9.15 (br, 1H), 8.82 (d, J = 4.8 Hz, 1H), 7.99−7.93 (m, 1H) 7.88 (t, J = 8.2 Hz, 2H), 7.59−7.50 (m, 3H), 7.29 (d, J = 7.5 Hz, 1H), 4.52−4.23 (m, 4H), 3.34−3.32 (m, 2H), 2.83−2.63 (m, 2H), 2.48−2.35 (m,

dx.doi.org/10.1021/ic401782x | *Inorg. Chem.* 2013, 52, 11480−11492

2H), 1.31 (s, 9H), 1.11 (t, J = 7.4 Hz, 3H); FTIR (KBr, cm^{-1}) 3423, 1653 ($\nu_{C=O}$), 1606, 1523, 1456, 1383, 1292, 1242 (ν_{NO3}), 1155, 1030 (ν_{NO3}), 916, 819, 765, 632.

Amide Methanolysis Reactivity of 4-ClO_4. *Product Identification.* To a methanol solution of **4-ClO_4** (22 mg, 0.027 mmol) was added a methanol solution of $Me_4NOH{\cdot}5H_2O$ (5.0 mg, 0.027 mmol). The resulting cloudy mixture was stirred for 24 h at ambient temperature, after which time a water solution containing excess $Me_4NOH{\cdot}5H_2O$ (20 mg, 0.11 mmol) was added to the mixture and the resulting solution was stirred for 20 min. The organic products were extracted from this solution using CH_2Cl_2 (3 × 5 mL). The combined organic fractions were then dried over Na_2SO_4, filtered, and the solvent removed under vacuum. The resulting light yellow solid exhibited ^{1}H NMR features identical to those previously reported for *N*-((ethylthio)ethyl)-*N*-((6-amino-2-pyridyl)methyl)-*N*-((2-pyridyl)-methyl)amine (eappa: 8.1 mg, 96% yield).[22] Me_4NClO_4 was isolated from the reaction mixture as previously described.[19] The methyltrimethylacetate produced in the amide methanolysis reaction of **4-ClO_4** was identified by ^{1}H NMR (s, 1.13 ppm) and was quantified (1 equiv) via integration of this signal versus the internal standard triphenylmethane.

Reaction of 4-ClO_4 with $Me_4NOH{\cdot}5H_2O$. *Characterization of 4′-ClO_4.* To an acetonitrile solution of $Me_4NOH{\cdot}5H_2O$ (9.8 mg, 0.054 mmol) was added methanol (2 drops) to enhance dissolution of the salt. A separate solution of **4-ClO_4** (43 mg, 0.054 mmol) was prepared in acetonitrile (~2 mL). Admixture of these solutions produced a light yellow solution containing a precipitate. Following removal of the solvent under vacuum, the remaining solid was dissolved in CH_2Cl_2 and was filtered though a Celite/glass wool plug. The filtrate was collected, and the solvent was removed under vacuum. ^{1}H NMR (CD_3CN, 300 MHz) δ 8.80 (br, 1H), 8.68 (d, J = 4.9 Hz, 1H), 7.94–7.87 (m, 2H), 7.61–7.56 (m, 2H), 7.45 (t, J = 6.0 Hz, 1H), 7.36 (d, J = 7.5 Hz, 1H), 4.31 (br, 2H), 4.27 (br, 2H), 3.15 (br, 2H), 2.65 (t, J = 6.5 Hz, 2H), 2.41(q, J = 7.4 Hz, 2H), 1.26 (s, 9H), 1.12 (t, J = 7.4 Hz, 3H); FT-IR (KBr, cm^{-1}) 3354 (br), 1658 ($\nu_{C=O}$), 1606, 1528, 1521, 1455, 1406, 1300, 1159 (ν_{ClO4}), 1092 (ν_{ClO4}), 1002 (ν_{ClO4}), 914 (ν_{ClO4}), 803, 764, 620 (ν_{ClO4}).

Kinetic Studies. ^{1}H NMR kinetic studies of the amide methanolysis reaction of **4-ClO_4** were performed using a JEOL ECX-300 NMR with a thermostatted probe. A temperature calibration curve for the range of 220 to 295 K was obtained using ethylene glycol. Data collection was performed using a method analogous to that used to obtain rate data for the amide methanolysis reaction of [(epppa)Zn]$(ClO_4)_2$ (**3-ClO_4**).[22] At regular intervals, the integrated intensity of the *t*-butyl methyl signal (1.27 ppm) was determined via automatic integration available on the Delta NMR Processing and Control Software (version 4.3.6) and normalized through comparison against the integrated intensity of the internal standard $CHPh_3$ (5.56 ppm). Pseudo-first order rate constants were determined from the slopes of ln[**4′-ClO_4**] versus time. Data in these plots represent more than three half-lives and typical correlation coefficients for these plots were ≥0.992. Second order rate constants were determined using the known concentration of CD_3OD in the mixture.[32] Variable concentration studies in terms of CD_3OD (0.21 to 15.39 M) for the amide methanolysis reaction of **4-ClO_4** revealed saturation-type kinetics with respect to the alcohol. Similar studies for the amide methanolysis reaction of **3-ClO_4** revealed a linear relationship. An Eyring plot was constructed for the amide methanolysis reaction of **4-ClO_4** using rate constants over a range of 21 °C (274–295 K). All data used in the Eyring plot was collected in triplicate with [CD_3OD] = 15.39 M in CD_3CN.

Solvent Kinetic Isotope Effect Studies. The influence of solvent-derived protons was explored through the comparative use of CD_3OD and CD_3OH in kinetic studies of the amide methanolysis reactions of **3-ClO_4** and **4-ClO_4**. The experimental procedure for CD_3OD is described above. An identical approach was used with CD_3OH with the exception of the presence of 4 equiv of $CHPh_3$ as an internal standard. All reactions were carried out at 295 K and [CD_3OH] = 15.39 M in CD_3CN. All data used to examine the solvent kinetic isotope effect were carried out in triplicate.

X-ray Crystallography. A crystal of **4-NO_3** was mounted on a glass fiber using a viscous oil and was transferred to a Nonius Kappa CCD diffractometer with Mo Kα radiation (λ = 0.71073 Å) for data collection at 150(1) K. Methods for the determination of cell constants and unit cell refinement have been previously described.[19] The structure was solved by a combination of direct methods and heavy atom methods using SIR97.[33] All of the non-hydrogen atoms were refined with anisotropic displacement coefficients. Hydrogen atoms were assigned isotropic displacement coefficients U(H) = 1.2U(C) or 1.5$U(C_{methyl})$, and their coordinates were allowed to ride on their respective carbons using SHELXL97.[34]

Computational Methods. All calculations were performed using the Gaussian 09 program package.[35] The geometries of reactants, intermediates, transition states, and products were optimized in the gas phase at the B3LYP/Lanl2dz level of theory without any symmetry constraints using the corresponding Hay–Wadt effective core potential (ECP) for zinc and lead.[36−38] The final energies of the optimized structures were further improved by performing single point calculations including additional d and p polarization functions for O (α = 0.96), N (α = 0.74), C (α = 0.59), and H (α = 0.36) atoms (taken from the EMSL's Gaussian basis set library), respectively, in the basis set used for optimizations. Hessians were calculated at the same level of theory as the optimizations to confirm the nature of the stationary points along the reaction coordinate. The transition states were confirmed to have only one negative eigenvalue corresponding to the reaction coordinates. In this paper, the energies obtained at the B3LYP/{Lanl2dz + d (O, N, and C) + p (H)}/ including thermal corrections are discussed.

RESULTS

Preparation and Characterization of [(epppa)Pb(X)$_2$] (X = ClO_4^- or NO_3^-). *Synthesis.* Treatment of epppa with an equimolar amount $Pb(ClO_4)_2{\cdot}3H_2O$ or $Pb(NO_3)_2$ in methanol enabled the generation of [(epppa)Pb(X)$_2$] (**4-X**). Precipitation of the perchlorate salt using Et_2O resulted in the isolation of analytically pure **4-ClO_4**, which was characterized by elemental analysis, ^{1}H and ^{13}C NMR, IR, and conductivity measurements. A similar isolation procedure yielded **4-NO_3**, which was characterized by ^{1}H NMR, IR, and X-ray crystallography.

X-ray Crystallographic Characterization of 4-NO_3. A thermal ellipsoid view of **4-NO_3** is shown in Figure 1(left). Details of the X-ray data collection and refinement for **4-NO_3** are given in Table 1. Selected bond angles for this complex are given in Table 2. The overall coordination number of the Pb(II) center in **4-NO_3** is nine, with each nitrate anion coordinated in a bidentate fashion to give an overall holodirected-type structure.[39] The epppa chelate ligand is κ^5-

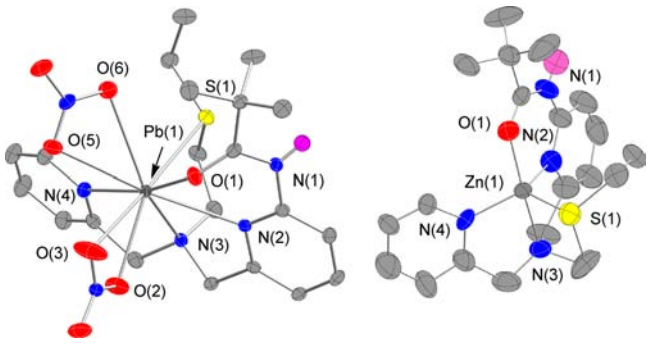

Figure 1. Thermal ellipsoid representations of **4-NO_3** (left) and the cationic portion of **3-ClO_4** (right). Ellipsoids are drawn at the 50% probability level. Hydrogen atoms, except the amide proton, have been omitted for clarity.

Table 1. Summary of X-ray Data Collection and Refinement[a]

	4-NO_3
empirical formula	$C_{21}H_{30}N_6O_7PbS$
formula weight	717.76
crystal system	monoclinic
space group	$P\ 2_1/n$
a (Å)	10.70150(1)
b (Å)	15.6611(2)
c (Å)	15.8963(2)
a (deg)	90
b (deg)	100.3770(8)
c (deg)	90
V (Å^3)	2620.60(5)
Z	4
density (calcd), Mg m^{-3}	1.819
temp (K)	150(1)
crystal size (mm)	0.18 × 0.15 × 0.10
diffractometer	Nonius KappaCCD
abs. coeff. (mm^{-1})	6.569
2θ max (deg)	54.96
completeness to 2θ (%)	99.9
reflections collected	11303
indep. reflections	6011
variable parameters	330
$R1/wR2$[b]	0.0237/0.0455
goodness-of-fit (F^2)	1.061
largest diff. (e Å^{-3})	1.802/-0.671

[a]Radiation used: Mo Kα (λ = 0.71073 Å). [b]$R1 = \sum||F_o| - |F_c||/\sum|F_o|$; $wR2 = [\sum[w(F_o^2 - F_c^2)^2]/[\sum(F_o^2)^2]]^{1/2}$ where $w = 1/[\sigma^2(F_o^2) + (aP)^2 + bP]$.

Table 2. Selected Bond Distances (Å) and Angles (deg) for 4-NO_3[a]

Pb(1)−O(1)	2.645(2)	O(1)−Pb(1)−N(4)	167.56(7)
Pb(1)−N(2)	2.749(2)	O(1)−Pb(1)−N(2)	65.65(7)
Pb(1)−N(3)	2.720(2)	N(4)−Pb(1)−N(2)	125.89(7)
Pb(1)−N(4)	2.607(3)	O(1)−Pb(1)−N(3)	127.08(7)
Pb(1)−S(1)	3.0619(8)	N(4)−Pb(1)−N(3)	64.90(8)
Pb(1)−O(2)	2.592(2)	N(2)−Pb(1)−N(3)	61.53(7)
Pb(1)−O(3)	2.845(3)	N(3)−Pb(1)−S(1)	69.04(6)
Pb(1)−O(5)	2.912(2)	O(1)−Pb(1)−S(1)	99.26(5)
Pb(1)−O(6)	2.864(2)	N(4)−Pb(1)−S(1)	81.48(6)
		N(2)−Pb(1)−S(1)	73.36(5)

[a]Estimated standard deviations in the last significant figure are given in parentheses.

coordinated by the N_3S-donor set along with the amide oxygen atom. The Pb−N(chelate) distances found in **4-NO_3** (2.607(2)−2.749(2) Å) are similar to the ranges found in Pb(II) complexes of N_4-donor chelate ligands ([(H_2tpaa)Pb−Cl] (2.646(6)−2.803(6) Å),[40] [(TQA)Pb(NO_3)$_2$] (2.549(3)−2.680(3) Å),[41] and [(6-Me_3TPA)Pb(NO_3)]NO_3 (2.546−2.677 Å)).[42] The Pb(II)-S(thioether) distance of 3.0619(8) Å is similar to the distances found in other Pb(II) thioether-containing structures (e.g., [Pb([18]aneO_4S_2)(H_2O)$_2$(κ^2-BF_4)]BF_4, 3.0151(8), 3.0191(7) Å;[43] [Pb([18]aneO_4S_2)-(ClO_4)$_2$], 3.091(1) Å;[44] [Pb([18]aneO_4S_2)(NO_3)$_2$], 3.114(6), 3.131(6) Å;[44] [Pb([15]aneO_3S_2)$_2$](BF_4)$_2$, 3.022(2)−3.116(2) Å;[43] [Pb([9]aneS_3)$_2$(ClO_4)$_2$], avg 3.076 Å[45]). In terms of the amide coordination, the Pb(II)-O(amide) distance of 2.645(2) Å is significantly longer than M(II)-O(amide) bonds in Group 12 analogues supported by either the epppa (**3-ClO_4**: Zn−O(amide), 1.998(7) Å)[22] or the bmppa (*N*,*N*-bis(2-methylthio)ethyl-*N*-((6-pivaloylamido-2-pyridyl)methyl)amine; [(bmppa)Cd(ClO_4)]ClO_4: Cd−O(amide), 2.302(2) Å;[21] [(bmppa)Hg(ClO_4)]ClO_4: Hg−O(amide), 2.271(5) Å[46]) chelate ligands. The O(1)−M(1)−N(2)−C(6) torsion angle (−21.62°) is similar to that found in the Hg(II) complex [(bmppa)Hg(II)(ClO_4)]ClO_4 (−22.5°).[46] Overall, the average M-N distance, as well as the M-S(thioether) and M-O(amide) distances associated with chelate ligand coordination in **4-NO_3**, exceed those found in the zinc complex **3-ClO_4** by 0.63−0.68 Å. This is a result of the larger ionic radius (Pb(II) (1.19 Å); Zn(II) (0.74 Å))[47] as well as the higher coordination number of the Pb(II) complex. Finally, both nitrate ions are coordinated to the Pb(II) center in **4-NO_3** in a bidentate fashion, with the nitrate coordinated via O(5) and O(6) being nearly symmetric bidentate.[48]

Spectroscopic and Solution Conductivity Properties. The solid-state IR spectrum of **4-NO_3** contains vibrations at 1242 (ν_1) and 1030 (ν_2) cm^{-1}, which are consistent with the bidentate nitrate coordination identified via X-ray crystallography.[49] For the perchlorate analogue **4-ClO_4**, a series of four vibrations at ∼1163, 1096, 1018, and 918 cm^{-1} suggest bidentate coordination of the perchlorate anions.[49]

When dissolved in acetonitrile, **4-ClO_4** is a 1:2 electrolyte (Figure 2) which is consistent with the dissociation of both

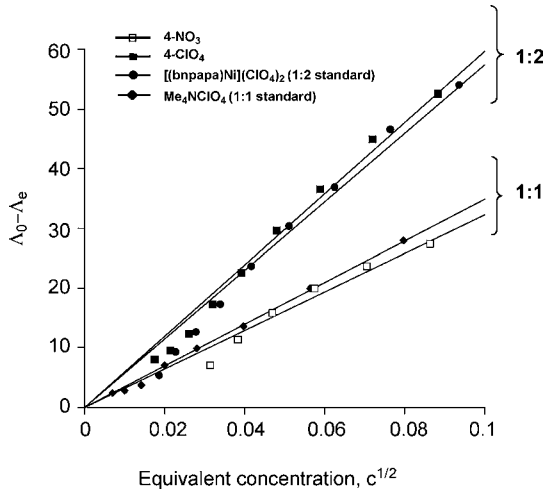

Figure 2. Onsager plot of conductivity data for **4-NO_3**, **4-ClO_4**, the 1:1 standard Me_4NClO_4, and the 1:2 standard [(bnpapa)Ni](ClO_4)$_2$ in acetonitrile.

perchlorate anions. These anions are likely replaced with coordinated solvent ligands in acetonitrile-containing solutions of the complex. The ^{1}H NMR spectrum of **4-ClO_4** in CD_3CN is shown in Figure 3a. The signals for the chelate ligand are shifted downfield relative to the free ligand and are sharp, with well-resolved ^{1}H−^{1}H coupling. These features are consistent with chelate ligand coordination to the Pb(II) center in a structure that is not fluxional on the NMR time scale. The appearance of four distinct doublets for the benzylic protons, as well as inequivalent protons for the methylene units of the thioether appendage, is consistent with retention of the chelate ligand coordination mode found in the solid state. Coupling between ^{207}Pb and the protons of the ligand could not be clearly identified in the ^{1}H NMR spectrum of **4-ClO_4**.

dx.doi.org/10.1021/ic401782x | Inorg. Chem. 2013, 52, 11480−11492

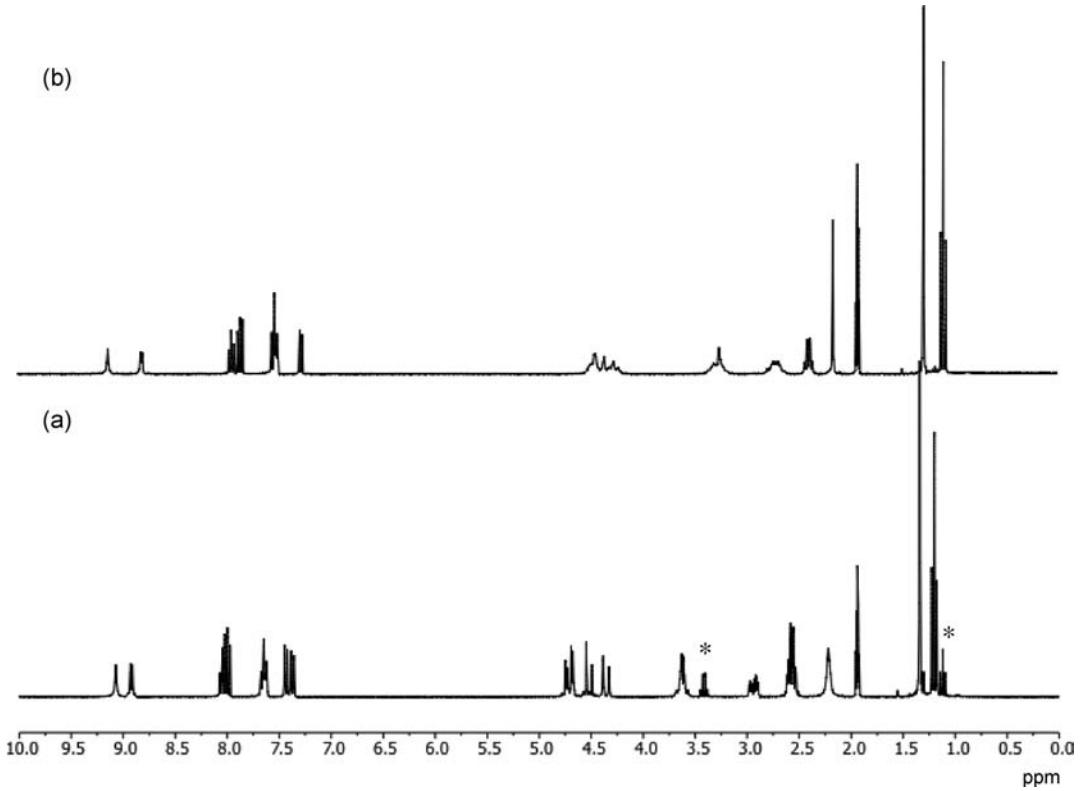

Figure 3. ^{1}H NMR spectral features of (a) **4-ClO$_4$** and (b) **4-NO$_3$** in CD_3CN at ambient temperature. The asterisks denote trace diethyl ether that was present in the ^{1}H NMR sample.

Scheme 2

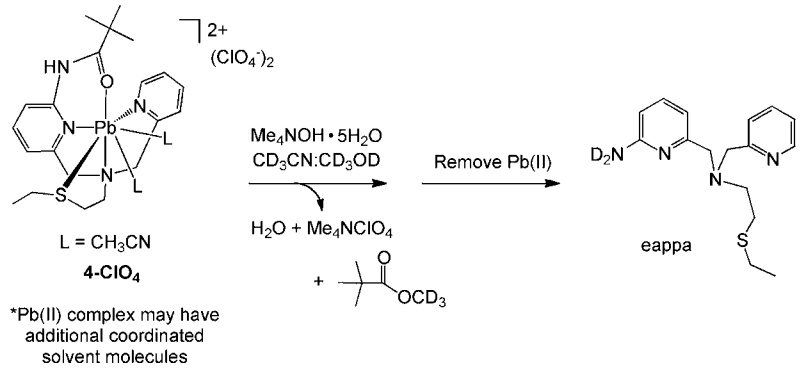

Notably, the ^{1}H NMR spectrum of **4-NO$_3$** differs in terms of the chemical shifts of several of the resonances (Figure 3b). Most notable is broadening and upfield shifts (relative to **4-ClO$_4$**) for the proton resonances of the benzylic positions and thioether appendage. Suspecting that this may indicate interactions between the Pb(II) center and the nitrate counterions,[2,43] we investigated **4-NO$_3$** via conductivity measurements (Figure 2). Unlike **4-ClO$_4$**, the nitrate analogue is not a 1:2 electrolyte, but instead exhibits 1:1 behavior, indicating that one of the two nitrate anions remains coordinated in acetonitrile solution. In the amide cleavage reactivity studies outlined below, we have only employed **4-ClO$_4$**.

Amide Cleavage Reactivity. *Product Identification.* We have previously reported that upon treatment with $Me_4NOH\cdot 5H_2O$ in CD_3CN:CD_3OD (3:5), **3-ClO$_4$** undergoes amide methanolysis as shown in Scheme 1c.[22] Treatment of **4-ClO$_4$** with $Me_4NOH\cdot 5H_2O$ in CD_3CN:CD_3OD (3:5) also results in amide cleavage (Scheme 2). The products of this reaction, including d_3-methyltrimethylacetate, were identified and quantified using approaches as previously described.[19,22] We have previously reported that exposure of free chelate ligands containing the 6-pivaloylamido group to $Me_4NOH\cdot 5H_2O$ in CD_3CN:CD_3OD (3:5) does not result in amide cleavage in the time required for completion of the amide methanolysis reactions of the divalent metal complexes.[21]

Kinetic Studies. Using methods previously employed for kinetic studies of the amide methanolysis reaction of **3-ClO$_4$**,[22] we collected rate data for the amide methanolysis reaction that occurs upon treatment of **4-ClO$_4$** with $Me_4NOH\cdot 5H_2O$ in CD_3CN:CD_3OD (3:5). Pseudo first-order rate constants (Table 3) were determined from slopes of plots of ln[**4′-ClO$_4$**] versus time. A typical correlation coefficient for these first-order plots was ≥0.992. At a given temperature, the

dx.doi.org/10.1021/ic401782x | *Inorg. Chem.* 2013, 52, 11480−11492

Table 3. Rate Constants for Amide Methanolysis Reaction of 4-ClO_4 in CD_3CN:CD_3OD (3:5)

temp (K)	4-ClO_4 (M)	[CD_3OD] (M)	k_{obs} (sec^{-1})
295	0.020	15.39	$8.07(43) \times 10^{-4}$
288	0.020	15.39	$4.98(34) \times 10^{-4}$
281	0.020	15.39	$2.47(21) \times 10^{-4}$
274	0.020	15.39	$1.20(6) \times 10^{-4}$
295	0.020	9.23	$7.42(43) \times 10^{-4}$
295	0.020	0.92	$5.27(35) \times 10^{-4}$
295	0.020	0.21	$1.50(4) \times 10^{-4}$

observed rate of amide methanolysis was ~10-fold faster for the Pb(II) complex versus the Zn(II)-containing analogue.[22]

Examination of the rate of amide methanolysis as a function of the concentration of CD_3OD (0.21−15.39 M) in CD_3CN revealed additional differences between the reactions of **3-ClO_4** and **4-ClO_4**. Specifically, the rate of amide methanolysis for the zinc complex **3-ClO_4** exhibits a linear correlation with increasing methanol concentration (Figure 4), and therefore

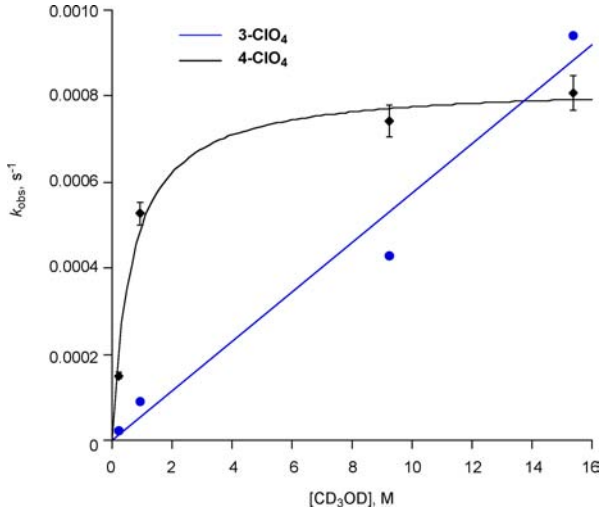

Figure 4. Plot of [CD_3OD] versus k_{obs} for the amide alcoholysis reactions of **3-ClO_4** and **4-ClO_4**. The saturation curve for **4-ClO_4** is fit according to eq 1.

overall second order behavior (rate = k[**3-ClO_4**][CD_3OD]). However, the Pb(II) complex **4-ClO_4** instead exhibits saturation behavior (Figure 4), indicating a reaction that is more complicated than a single step. The saturation behavior is consistent with a reaction pathway involving an equilibrium prior to an irreversible step having a rate constant k_2 as shown in eq 1. The calculated values of K_1 and k_2 from the fitting of this equation to the variable [CD_3OD] concentration data for **4-ClO_4** gave $K_1 = 1.5(4)$ and $k_2 = 8.3(5) \times 10^{-4}$ M^{-1} s^{-1}.

$$k_{obs} = \frac{k_2 k_1 [CD_3OD]}{1 + K_1 [CD_3OD]} \quad (1)$$

Eyring plots were constructed for the amide methanolysis reactions of **3-ClO_4** and **4-ClO_4** (Figure 5). Activation parameters derived from these plots are given in Table 4. This data reveals that the slightly faster rate of methanolysis for the Pb(II) complex **4-ClO_4** is associated with lower values of enthalpy and entropy of activation. Both complexes exhibit $\Delta S^{\ddagger}$ values that are consistent with an intramolecular rate-determining step.[20]

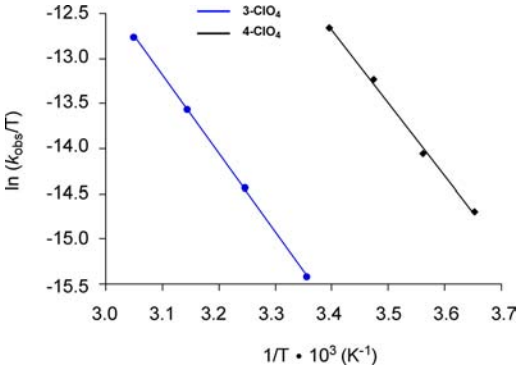

Figure 5. Erying plots for the amide methanolysis reactions of **3-ClO_4** and **4-ClO_4**.

Table 4. Thermodynamic Data for Amide Methanolysis Reactions of 3-ClO_4 and 4-ClO_4 in CD_3CN:CD_3OD (3:5)

	3-ClO_4[a]	4-ClO_4[b]
$\Delta H^{\ddagger}$ (kcal/mol)	17.3(2)	16.0(6)
$\Delta S^{\ddagger}$ (cal/(mol·K))	−24(1)	−17(2)
$T\Delta S^{\ddagger}$ (kcal/mol)[c]	−7.2(3)	−5.2(7)
$\Delta G^{\ddagger}$ (kcal/mol)[d]	24.5(5)	21.3(9)

[a]Reference 22. [b]This work. [c]298 K. [d]Calculated from $\Delta G = \Delta H - T\Delta S$.

Solvent kinetic isotope effect (SKIE) experiments using CD_3OD and CD_3OH revealed a SKIE (k^H/k^D) of 1.4 for the amide methanolysis reaction of **3-ClO_4**. By contrast, the amide methanolysis reaction of the Pb(II)-containing **4-ClO_4** shows no solvent kinetic isotope effect.

Evaluation of Possible Intermediates in the Amide Methanolysis Reactions. As we have previously reported, treatment of **3-ClO_4** with $Me_4NOH{\cdot}5H_2O$ in acetonitrile or a CD_3CN:CD_3OD (3:5) mixture initially results in the formation of a deprotonated amide species (**3′-ClO_4**, Scheme 3).[22] This complex has been isolated and characterized by ^1H and ^{13}C NMR, IR, and elemental analysis.[22] Unique ^1H NMR spectral features of this compound relative to the starting material include the absence of an N-*H* resonance and significant upfield shifts of the resonances associated with the *β*-protons of the amide-appended pyridyl ring (>0.45 ppm) and the *t*-butyl (0.22 ppm) protons. The upfield shifts of these resonances are consistent with enhanced electron density within the deprotonated amide unit, which is delocalized into the pyridyl ring.[19] Additionally, proton resonances associated with the thioether appendage are shifted upfield relative to their position in **3-ClO_4**. This change suggests a weakening of the Zn(II)-S(thioether) interaction in **3′-ClO_4**, which is supported by density functional theory (DFT) calculations reported herein (vide infra). In terms of IR features, **3′-ClO_4** does not exhibit a 1646 cm^{-1} vibration that is assigned to the coordinated amide carbonyl unit in the starting amide complex. Combined, these spectral features are consistent with the formation of a deprotonated amide species. Upon introduction of methanol, **3′-ClO_4** undergoes reaction to give amide methanolysis products, providing evidence that it is a viable intermediate in the amide methanolysis pathway of **3-ClO_4**.

Treatment of **4-ClO_4** with 1 equiv of $Me_4NOH{\cdot}5H_2O$ in acetonitrile or CD_3CN:CD_3OD (3:5) results in the initial formation of a new species, **4′-ClO_4**. This complex has a *t*-butyl ^1H NMR resonance that is shifted slightly upfield (0.09 ppm)

dx.doi.org/10.1021/ic401782x | Inorg. Chem. 2013, 52, 11480−11492

Scheme 3

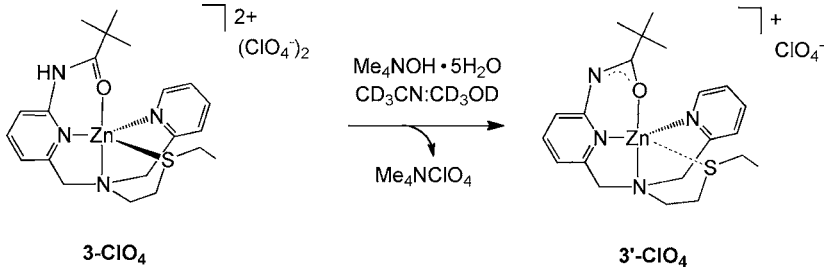

3-ClO$_4$ **3′-ClO$_4$**

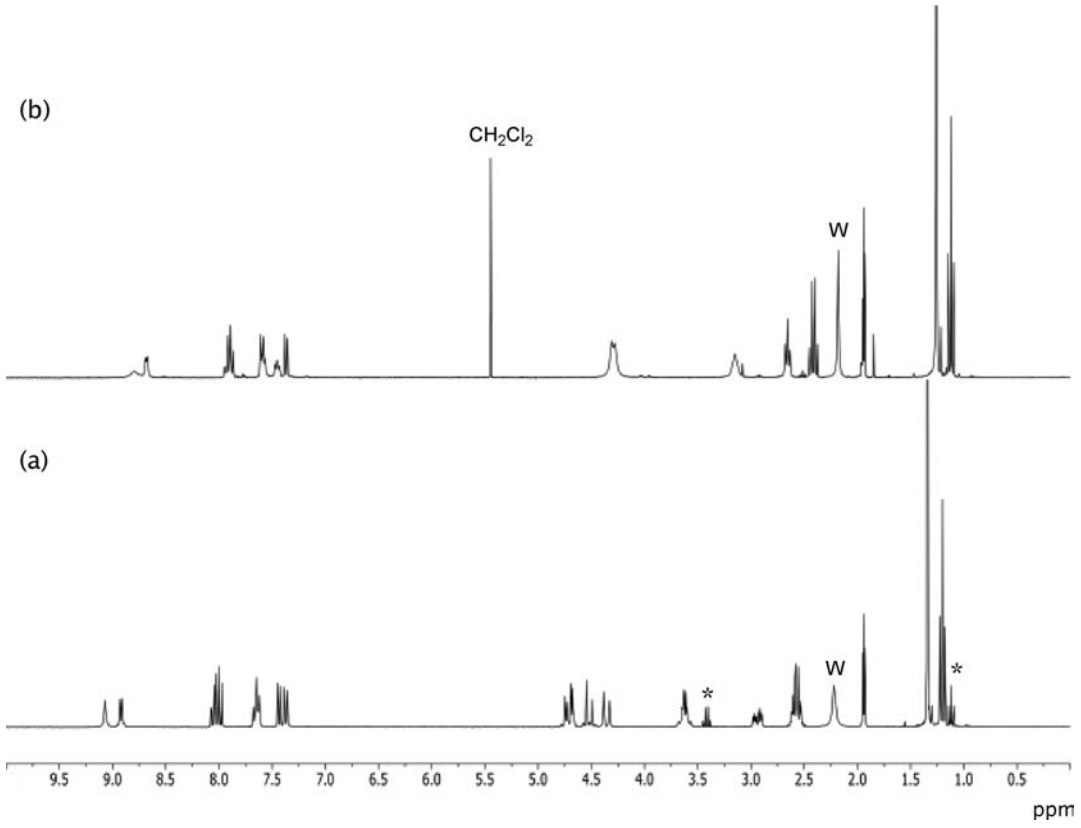

Figure 6. ^{1}H NMR spectral features of (a) **4-ClO$_4$** and (b) **4′-ClO$_4$** in CD_3CN at ambient temperature. The asterisks denote trace diethyl ether that was present in the ^{1}H NMR sample. Water and CH_2Cl_2 impurities are also denoted in the spectra.

Scheme 4

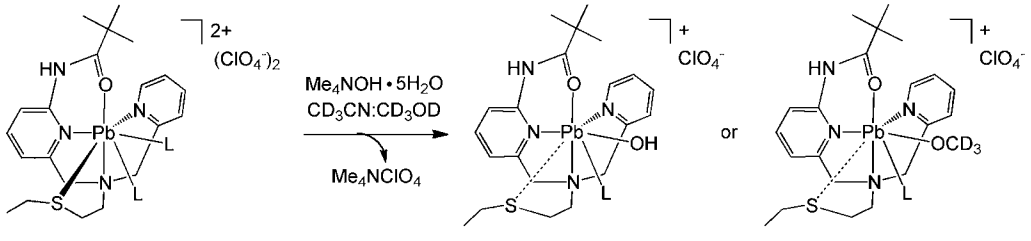

4-ClO$_4$ L = CD_3CN or CD_3OD Possible formulations for **4′-ClO$_4$** in CD_3CN/CD_3OD

relative to the chemical shift of the same resonance in the starting material, but does not exhibit significant upfield shifts for any other protons of the amide-appended pyridyl ring (Figure 6). A broad N−H resonance is present in the ^{1}H NMR spectrum of **4′-ClO$_4$** at ∼8.8 ppm. Combined, these results suggest that **4′-ClO$_4$** does not contain a deprotonated amide moiety. This conclusion is supported by the solid state IR spectral features of **4′-ClO$_4$** wherein an amide carbonyl stretching vibration is still present at ∼1658 cm^{-1}. A notable difference in the ^{1}H NMR spectrum of **4′-ClO$_4$** versus that of **4-ClO$_4$** is that the former shows significant changes in the multiplicity of signals for the methylene protons of the

dx.doi.org/10.1021/ic401782x | *Inorg. Chem.* 2013, 52, 11480−11492

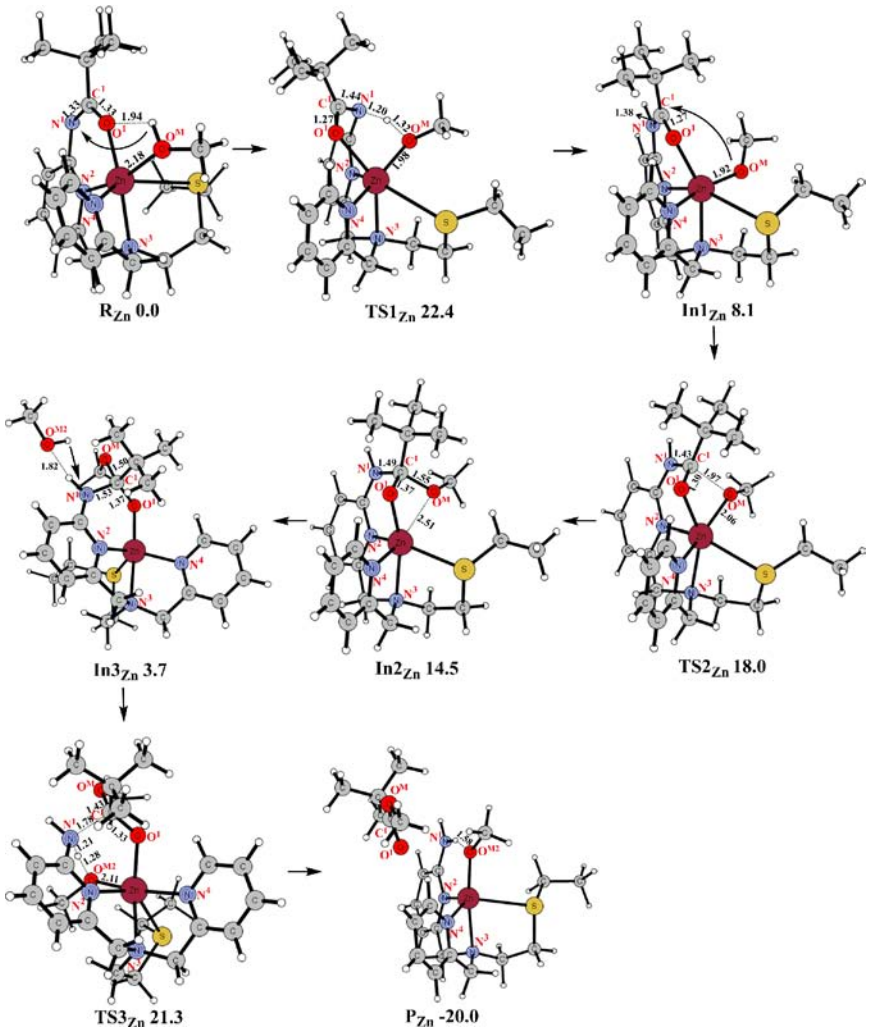

Figure 7. DFT-optimized structures of reactant, intermediates, transition states, and product in the amide methanolysis reaction pathway of **3-ClO$_4$**.

thioether appendage, which suggests a loss of diastereotopic character for these protons (Figure 6), perhaps due weakening or loss of the Pb(II)-S(thioether) interaction upon anion coordination. This change in the Pb(II)-S(thioether) interaction is supported by DFT calculations described herein (vide infra).

A possible structure for **4′-ClO$_4$** is an epppa-ligated Pb(II)-OH or Pb(II)-OCD$_3$ species (Scheme 4). Evidence for a mixture of such species in the amide methanolysis reaction of **4-ClO$_4$** is the formation of a small amount of amide hydrolysis product (identified via a trimethylacetate *t*-butyl resonance at 0.96 ppm; verified via treatment of **4-ClO$_4$** with CD$_3$CN:D$_2$O (3:5) which results in exclusively this hydrolysis product). Importantly, treatment of isolated **4′-ClO$_4$** with CD$_3$OD results in amide methanolysis, providing evidence that this compound is a viable intermediate in the amide methanolysis reaction pathway.

Computational Studies. The amide methanolysis pathways of **3-ClO$_4$** and **4-ClO$_4$** were modeled using density functional theory (DFT) calculations to correlate computed energetics with the results of the kinetic studies described above, as well as to provide insight into the mechanisms. Structures of geometry optimized reactants, transition states, and intermediates in the respective amide cleavage pathways of **3-ClO$_4$** and **4-ClO$_4$** are provided in Figures 7 and 8, respectively. Table 5 lists the M(II)/chelate ligand bond distances in each of these structures. The potential energy surface (PES) diagrams of these pathways are shown in Figure 9. The starting reactant complex for the calculated pathway of each metal ion is a deprotonated amide species containing a coordinated methanol, [(epppa$^-$)Zn(CH$_3$OH)]$^+$ (**R$_{Zn}$**) and [(epppa$^-$)Pb(CH$_3$CN)$_2$(CH$_3$OH)]$^+$ (**R$_{Pb}$**). **R$_{Zn}$** was developed from the X-ray structural data of [(epppa)Zn](ClO$_4$)$_2$ (**3-ClO$_4$**),[22] followed by geometry optimization for a structure that exhibits amide deprotonation and methanol coordination. **R$_{Pb}$** was developed from the X-ray crystallographic data of **4-NO$_3$**. Two molecules of coordinated acetonitrile were found to optimally model the solvated form of the [(epppa)Pb]$^{2+}$ cation based on comparisons to the X-ray crystallographically determined bond distances involving the epppa chelate ligand in **4-NO$_3$**. The structure of [(epppa$^-$)Pb-(CH$_3$CN)$_2$(CH$_3$OH)]$^+$ (**R$_{Pb}$**, Figure 8), wherein the amide has been deprotonated and a coordinated methanol has been added, was then geometry optimized.

In the optimized structure of the deprotonated amide Zn(II) reactant complex (**R$_{Zn}$**), the coordinated methanol molecule interacts with coordinated amide oxygen via a hydrogen bond (Figure 7). This structure contains a six-coordinate Zn(II) center. The coordination number of the Zn(II) ion is 5 or 6 throughout the reaction pathway. The long Zn−S(thioether)

dx.doi.org/10.1021/ic401782x | *Inorg. Chem.* 2013, 52, 11480−11492

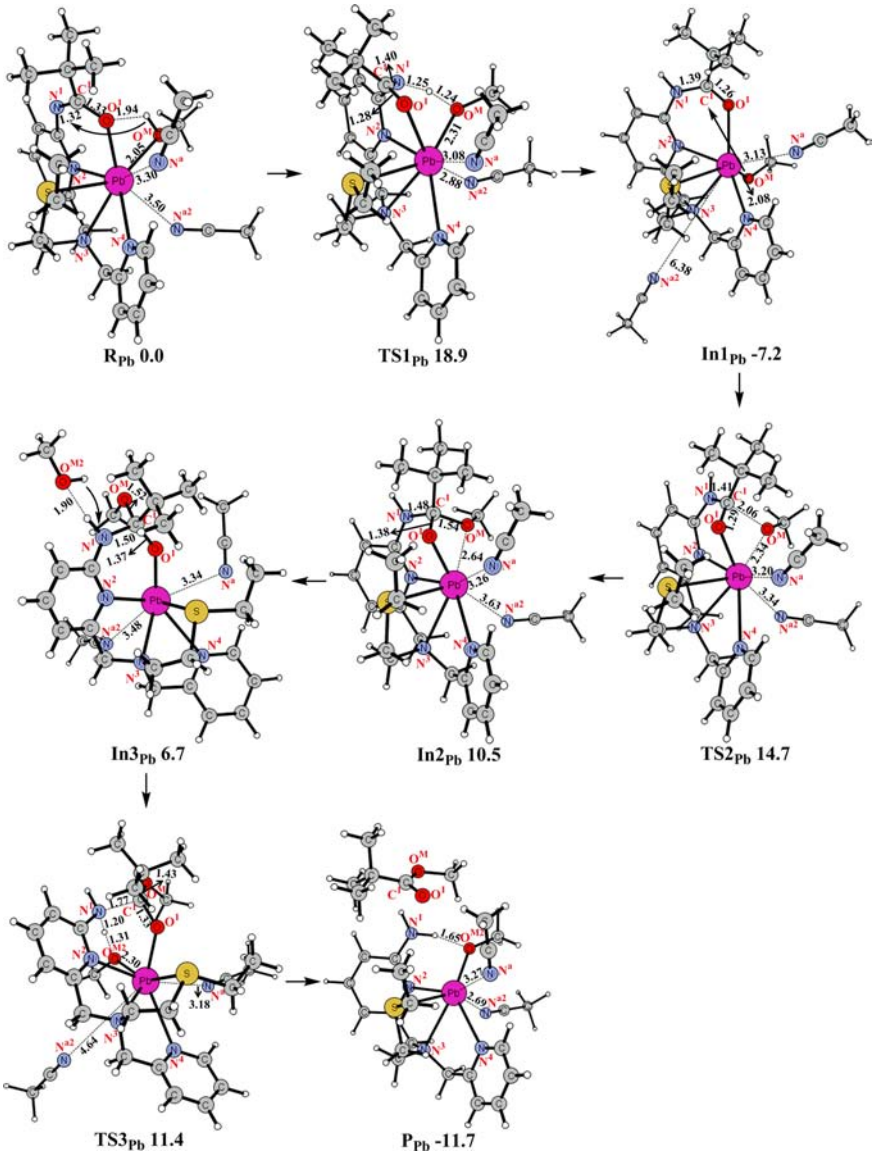

Figure 8. DFT-optimized structures of reactant, intermediates, transition states, and product in the reaction pathway leading to amide methanolysis of **4-ClO$_4$**.

distance (3.01 Å) in $\mathbf{R}_{Zn}$ suggests a weak interaction as, while it is within the sum of the van der Waals radii (3.19 Å) of the two atoms, the observed distance is >0.7 Å longer than that found in **3-ClO$_4$**. This elongation of the Zn(II)-S(thioether) interaction is consistent with the ^{1}H NMR features of the thioether appendage of **3′-ClO$_4$** as discussed above. The other zinc-ligand distances in $\mathbf{R}_{Zn}$ are generally elongated to a lesser extent (<0.3 Å) upon amide deprotonation and introduction of the anionic charge into the metal coordination environment. The first transition state investigated was for proton transfer from the coordinated methanol to the deprotonated amide of the chelate ligand. This step proceeds with an activation barrier of 22.4 kcal/mol to give $\mathbf{In1}_{Zn}$, a structure containing a neutral amide and a coordinated methoxide anion. This intermediate is endergonic by 8.1 kcal/mol relative to $\mathbf{R}_{Zn}$. The Zn(II)-chelate ligand distances in $\mathbf{In1}_{Zn}$ are slightly elongated relative to $\mathbf{R}_{Zn}$ (Table 5). Nucleophilic attack of the methoxide ligand on the amide carbonyl carbon results in the formation of the tetrahedral intermediate $\mathbf{In2}_{Zn}$. Notably, this transformation results in a decrease in the Zn−S(thioether) distance to 2.69 Å. Comparison of the amide C−N bond distances in $\mathbf{In2}_{Zn}$ (1.49 Å) and $\mathbf{In1}_{Zn}$ (1.38 Å) reveals elongation that is favorable for the subsequent amide cleavage step. A second molecule of methanol that is required for amide cleavage was then added to $\mathbf{In2}_{Zn}$ to form $\mathbf{In3}_{Zn}$. In the optimized structure of $\mathbf{In3}_{Zn}$, the additional methanol interacts with the amide N−H via a hydrogen bond (Figure 7). From $\mathbf{In3}_{Zn}$, which is endergonic by 3.7 kcal/mol relative to $\mathbf{R}_{Zn}$, proton transfer from methanol to the amide nitrogen leads to cleavage of the amide C−N bond. This transformation happens with a barrier of 17.6 kcal/mol from $\mathbf{In3}_{Zn}$ and an overall barrier of 21.3 kcal/mol from $\mathbf{R}_{Zn}$. In the final product ($\mathbf{P}_{Zn}$), the Zn(II) center coordinates a methoxide anion and is supported by the primary amine-containing chelate ligand (eappa). One equivalent of a noncoordinated carboxyl ester (methyltrimethylacetate) is also generated.

Similar to the X-ray structure of **4-NO$_3$**, the geometry optimized structure of the deprotonated amide Pb(II) reactant complex ($\mathbf{R}_{Pb}$) exhibits coordination of the chelate ligand with coordination space available for the binding of two solvent

dx.doi.org/10.1021/ic401782x | *Inorg. Chem.* 2013, 52, 11480−11492

Table 5. Structural Data for DFT-Calculated Structures (Å)

complex	M-S	M-N_4	M-N_2	M-N_3	M-O_1
[(epppa)Zn]$(ClO_4)_2$[a]	2.399(3)	1.983(8)	2.0470(16)	2.169(8)	1.998(7)
R_{Zn}	3.01	2.14	2.09	2.29	2.01
$TS1_{Zn}$	3.19	2.11	2.10	2.36	2.36
$In1_{Zn}$	3.12	2.15	2.24	2.27	2.17
$TS2_{Zn}$	2.86	2.13	2.16	2.36	2.10
$In2_{Zn}$	2.69	2.12	2.12	2.33	1.97
$In3_{Zn}$	2.67	2.10	2.07	2.34	1.93
$TS3_{Zn}$	2.83	2.18	2.17	2.39	2.05
P_{Zn}	2.74	2.11	2.11	2.32	1.93
[(epppa)Pb$(NO_3)_2$][b]	3.0619(8)	2.607(2)	2.749(2)	2.720(2)	2.645(2)
R_{Pb}	3.11	2.91	2.48	2.74	2.31
$TS1_{Pb}$	3.30	2.90	2.56	2.95	2.81
$In1_{Pb}$	3.59	2.60	2.78	2.62	2.71
$TS2_{Pb}$	3.26	3.06	2.57	2.96	2.29
$In2_{Pb}$	3.05	3.00	2.54	2.86	2.19
$In3_{Pb}$	3.07	2.93	2.46	2.74	2.14
$TS3_{Pb}$	3.36	3.08	2.62	3.02	2.23
P_{Pb}	3.38	2.86	2.56	2.86	2.19

[a]Ingle, G. K.; Makowska-Grzyksa, M. M.; Szajna-Fuller, E.; Sen, I.; Price, J. C.; Arif, A. M.; Berreau, L. M. *Inorg. Chem.* **2007**, *46*, 1471−1480. [b]This work.

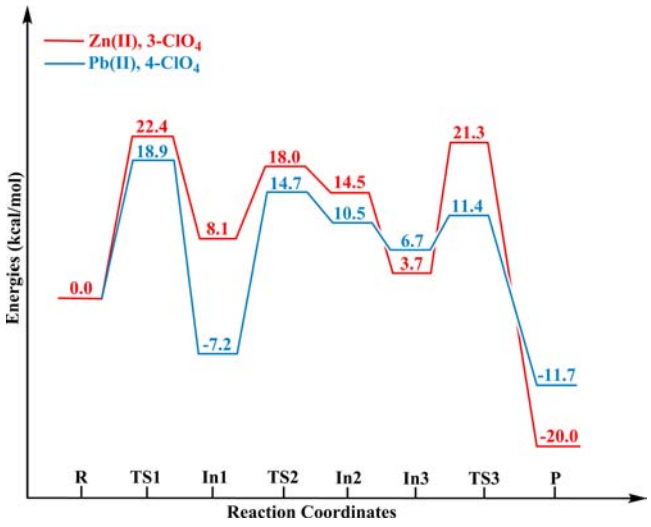

Figure 9. Free energy profiles for the amide methanolysis reactions for **3-ClO_4** and **4-ClO_4**.

molecules. The coordination number of the Pb(II) ion is 7 or 8 throughout the reaction pathway. Proton transfer to the deprotonated amide from a coordinated methanol occurs in this case with an activation barrier of 18.9 kcal/mol to give **$In1_{Pb}$**. This intermediate is 7.2 kcal/mol exergonic relative to **R_{Pb}**. The structure of **$In1_{Pb}$** contains a neutral, coordinated amide as well as a coordinated methoxide anion. The Pb(II)-S(thioether) distance in **$In1_{Pb}$** is 3.59 Å which, while within the sum of the van der Waals radii of the two atoms, represents a significant elongation relative to the same interaction in **R_{Pb}** (3.11 Å). Notably, the elongation of the Pb(II)-S(thioether) interaction in **$In1_{Pb}$** is consistent with the observed changes in the ^{1}H NMR spectral features of the thioether appendage of **4′-ClO_4** versus the starting **4-ClO_4** complex. Nucleophilic attack of the methoxide at the amide carbonyl carbon occurs with a barrier of 21.9 kcal/mol from **$In1_{Pb}$** and 14.7 kcal/mol relative to **R_{Pb}**. The intermediate formed, **$In2_{Pb}$**, is 10.5 kcal/mol endergonic relative to **R_{Pb}**. As was seen in the Zn(II) system, the Pb−S(thioether) interaction is stronger in **$In2_{Pb}$** (3.05 Å) and the C−N bond is elongated in **$In2_{Pb}$** (1.48 Å) relative to **$In1_{Pb}$** (1.39 Å). Once again, a second molecule of methanol required for amide cleavage was added to **$In2_{Pb}$** to form **$In3_{Pb}$**. In the optimized structure of **$In3_{Pb}$**, the additional methanol interacts with the amide N−H via a hydrogen bond (Figure 8). From **$In3_{Pb}$**, which is endergonic by 6.7 kcal/mol relative to **R_{Pb}**, proton transfer from methanol to the amide nitrogen leads to cleavage of the amide C−N bond. This transformation happens with a barrier of 4.7 kcal/mol from **$In3_{Pb}$** and an overall barrier of 11.4 kcal/mol from **R_{Pb}**. In the final product (**P_{Pb}**), the Pb(II) center coordinates a methoxide anion and is supported by the primary amine-containing chelate ligand (eappa). One equivalent of a noncoordinated carboxyl ester (methyltrimethylacetate) is also generated.

Based on the observation of small amounts of amide hydrolysis product in the amide methanolysis reaction of **4-ClO_4**, we also used DFT calculations to examine the relative energies of the Pb(II)-OCH_3 species (**$In1_{Pb}$**) and a Pb(II)−OH analogue. We found that the hydroxide compound is only 1.04 kcal/mol lower in energy in the gas phase, suggesting that these two compounds can form an acid/base equilibrium (Figure 10). Notably, the calculated free energy difference between these two compounds matches well with that derived for the equilibrium component in the saturation kinetics of the amide methanolysis of **4-ClO_4** (0.2 kcal/mol).

■ DISCUSSION AND CONCLUSIONS

Amide cleavage reactions catalyzed by enzymes containing a mononuclear zinc center are well-known in biological systems.[50] Though Pb(II) substitution for the active site zinc center has not been reported for an amide hydrolase to date, the general properties introduced by heavy metal substitution into zinc proteins is of current interest.[11] The amide hydrolysis reactivity of Zn(II) in biological systems is often proposed to involve the formation of a Zn(II)−OH nucleophile.[20] The involvement of Pb(II)−OH as a general base catalyst in tRNA

dx.doi.org/10.1021/ic401782x | *Inorg. Chem.* 2013, 52, 11480−11492

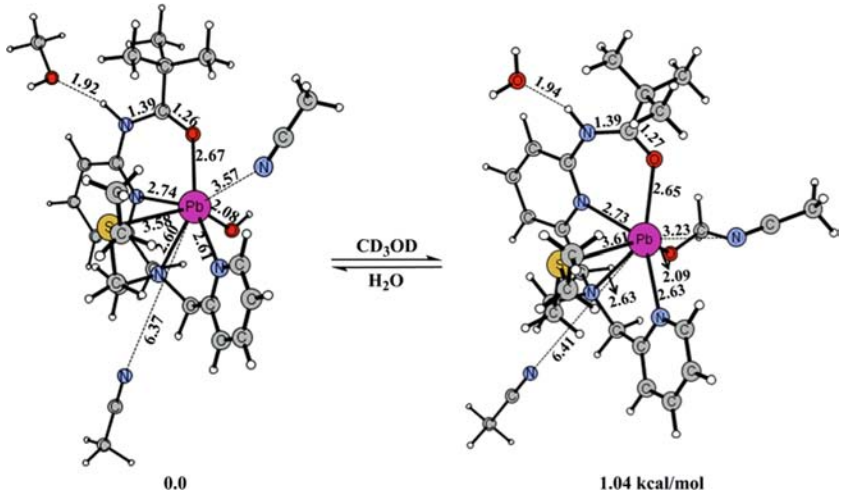

Figure 10. DFT optimized structures of $\mathbf{In1}_{Pb}$ (right) and a Pb−OH analogue and the equilibrium that relates these compounds.

hydrolysis has been proposed,[51,52] as well as a Pb(II)−OH acting as a nucleophile in the hydrolysis of uridine 2′,3′-cyclic monophosphate.[53] In the experiments described herein, we have examined in detail the coordination chemistry and amide methanolysis reaction pathways of mononuclear Pb(II) and Zn(II) complexes of an amide-appended chelate ligand.

Pb(II) and Zn(II) differ in a number of important ways. First, the ionic radius for the former is considerably larger (Pb(II) 1.19 Å; Zn(II) 0.74 Å).[47] This is reflected in the higher coordination numbers that are typically found for Pb(II) complexes versus Zn(II) analogues, including compound **4-NO$_3$** versus **3-ClO$_4$**, which exhibit overall coordination numbers in the solid state of nine and five respectively.[22] In both of these compounds, the epppa chelate ligand is coordinated in a κ^5-fashion. However, whereas the coordination of the chelate ligand in **4-NO$_3$** leaves available positions for anion or solvent coordination, in **3-ClO$_4$** the chelate ligand fully encapsulates the metal center. This is also the case for the geometry-optimized structures of the deprotonated amide species $\mathbf{R}_{Pb}$ and $\mathbf{R}_{Zn}$. As outlined below, we propose that it is this difference in accessibility of coordination positions at the Pb(II) center in **4-ClO$_4$** that enables a reaction pathway for amide cleavage in this complex that initially differs from that of the Zn(II) analogue **3-ClO$_4$**.

Pb(II) and Zn(II) are also similar in a number of important ways. According to Pearson's classification of hard and soft acids and bases, both are considered intermediate acids and therefore bind a variety of donor atoms.[54] In the X-ray crystal structures of **4-NO$_3$** and **3-ClO$_4$**, each metal ion binds a mixture of nitrogen, oxygen, and sulfur donors from the chelate ligand, with the Pb(II) complex exhibiting longer bond distances because of the larger size of the metal ion. The multidentate chelate nature of the epppa ligand ensures that the metal ion in **4-ClO$_4$** and **3-ClO$_4$** is not released during the transformations involved in amide cleavage.

Treatment of **4-ClO$_4$** or **3-ClO$_4$** with 1 equiv of $Me_4NOH\cdot 5H_2O$ in CD_3CN:CD_3OD (3:5) results in amide methanolysis and the formation of similar products. Thus, regardless of the divalent metal ion present, the same amide methanolysis products are obtained. Variable temperature kinetic studies of the reactions revealed only small differences in the activation parameters, with the $\Delta G^{\ddagger}$ for the Pb(II)-containing **4-ClO$_4$** being ∼3 kcal/mol lower than that found for the Zn(II) analogue **3-ClO$_4$**. However, differences in the influence of methanol concentration, saturation kinetics for **4-ClO$_4$** versus second-order behavior for **3-ClO$_4$**, and the identification of a small solvent deuterium kinetic isotope effect identified only for the reaction involving **3-ClO$_4$**, suggest differences in the reaction pathway. This led us to carefully investigate spectroscopically identifiable intermediates in the reaction pathways, as well as to examine the reaction as a function of metal ion via DFT calculations.

Upon introduction of 1 equiv of $Me_4NOH\cdot 5H_2O$ to acetonitrile solutions of **4-ClO$_4$** and **3-ClO$_4$** different isolable products are generated, as determined by ^{1}H NMR and IR. Whereas the Zn(II) complex **3-ClO$_4$** undergoes amide deprotonation to give **3′-ClO$_4$**, no evidence was identified for amide deprotonation in the Pb(II) analogue. Instead, the spectroscopic properties of the intermediate suggest the formation of a mixture of epppa-ligated Pb(II)-OH and Pb(II)-OCH_3 species containing a neutral amide. This difference in reactivity with $Me_4NOH\cdot 5H_2O$ is a consequence of the available coordination sites for anion binding in **4-ClO$_4$**, whereas anion coordination to **3-ClO$_4$** is considerably more difficult because of the more encapsulating chelate ligand coordination motif. This is reflected in the ∼15 kcal/mol difference in energy between $\mathbf{In1}_{Pb}$ and $\mathbf{In1}_{Zn}$.

DFT calculations indicate that both **4-ClO$_4$** and **3-ClO$_4$** may feasibly undergo amide methanolysis starting from a deprotonated amide species, with activation barriers for the rate-determining step that are generally consistent with experimentally determined free energies of activation. For example, for the Zn(II)-containing **3-ClO$_4$**, the rate-determining step would involve either protonation of the deprotonated amide, or protonation of the amine leaving group, as both steps have similar activation barriers (22.4 and 21.3 kcal/mol, respectively), which are similar to the experimentally determined free energy of activation ($\Delta G^{\ddagger}$ = 24.5 kcal/mol). We note that these activation barriers are also similar to the $\Delta G^{\ddagger}$ values recently reported for the methanolysis of an internal amide substrate in a Cu(II) complex.[55] The small observed normal SKIE identified for the reaction of **3-ClO$_4$** (1.4) may be consistent with intramolecular proton transfer from a coordinated methanol, or general acid assistance by a solvent molecule for departure of the leaving group.[55] General base assistance by a Zn(II)-OCH_3 moiety in accepting a proton from an exogenous solvent

dx.doi.org/10.1021/ic401782x | Inorg. Chem. 2013, 52, 11480−11492

Scheme 5

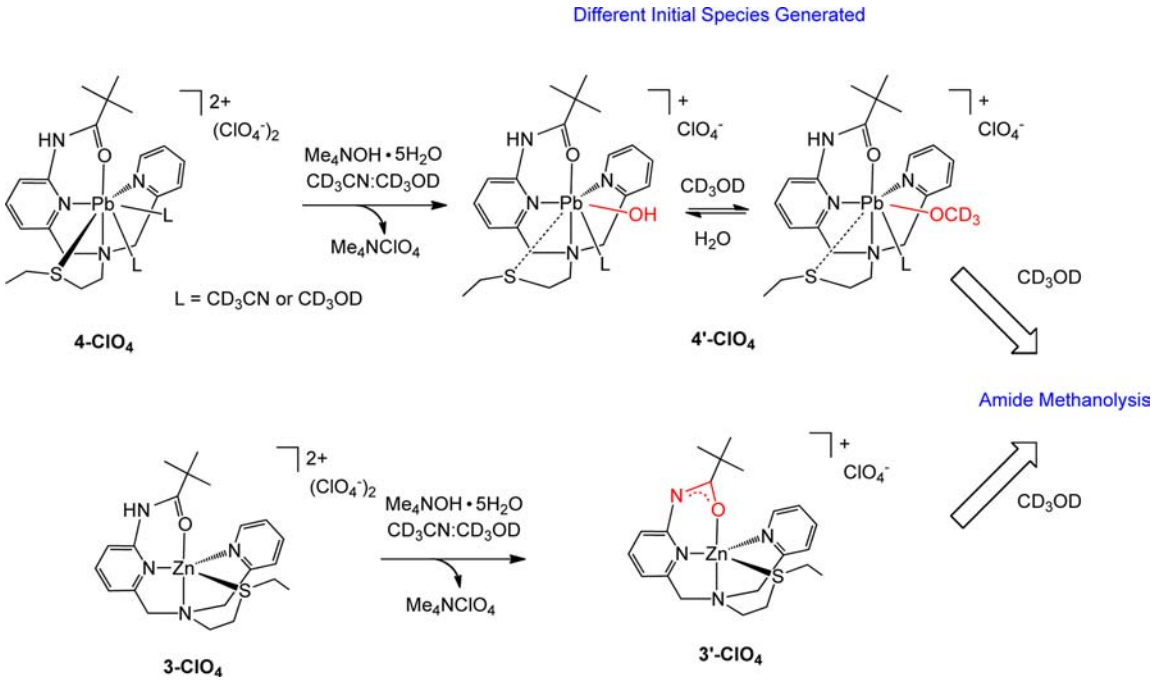

molecule that would nucleophilically attack the carbonyl would be expected to exhibit a larger SKIE.[56]

The DFT studies indicate that the reaction of Pb(II)-containing **4-ClO$_4$** starting from a deprotonated amide species ($\mathbf{R_{Pb}}$) would involve rate-limiting amide protonation from a coordinated methanol, a reaction with a calculated activation barrier of 18.9 kcal/mol. This value is comparable to the experimentally determined free energy of activation (21.3 kcal/mol). However, based on the lack of evidence for the initial formation of a deprotonated amide species in the reaction of **4-ClO$_4$** upon treatment with $Me_4NOH{\cdot}5H_2O$, we propose that this reaction proceeds via the direct formation of a Pb(II)−OH species $[(epppa)Pb{-}OH(sol)_n]^+$ (sol = CH_3CN or CH_3OH; n = 1−2), that equilibrates with a corresponding Pb(II)-OCH_3 ($\mathbf{In1_{Pb}}$) species. The equilibration of these two compounds is consistent with the observed saturation kinetic data wherein the Pb(II)−OH/Pb(II)-OCH_3 equilibrium precedes nucleophilic attack of the methoxide on the coordinated amide. The calculated activation barrier associated with this nucleophilic attack ($\mathbf{In1_{Pb}} \rightarrow \mathbf{TS2_{Pb}}$, 21.9 kcal/mol) is a very good match with the experimentally determined activation barrier (21.3 kcal/mol). The lack of an observed SKIE is consistent with this step being rate-determining, as no proton is in flight.[56]

Therefore, we propose that the amide methanolysis reactions of **3-ClO$_4$** and **4-ClO$_4$**, while giving the same products, proceed via different initial reactants, **3′-ClO$_4$** (modeled as $\mathbf{R_{Zn}}$) and **4′-ClO$_4$** (modeled as $\mathbf{In1_{Pb}}$) that are the result of the differences in the size and coordination preferences of Zn(II) versus Pb(II) (Scheme 5). That being said, in both cases the metal center is likely playing multiple roles in the amide cleavage reaction. These include electrophilic activation of the carbonyl via coordination of the oxygen atom and stabilization of the nucleophile.[57,58] In terms of Pb(II), our calculations indicate that the larger Pb(II) ion more effectively stabilizes the double Lewis activated structure having both amide and nucleophile coordination ($\mathbf{In1_{Pb}}$). Notably, the Pb(II) center also substantially lowers the activation barrier for leaving group departure, relative to the Zn(II) analogue (Figure 9). These effects likely relate to a more flexible metal coordination environment for Pb(II), wherein a greater range of metal−ligand distances may be accessed during the amide cleavage reaction.[59]

Overall, the purpose of this study was to evaluate how the presence of Pb(II) versus Zn(II) would influence an amide cleavage reaction. Our results indicate that Pb(II) may serve as a Lewis acid to promote amide cleavage and lower the energy barrier for key steps in the reaction pathway. The differences in the reaction pathway as compared to a Zn(II) analogue relate to the inherent chemical properties of this heavy metal ion.

■ ASSOCIATED CONTENT

Supporting Information

Analysis of solid-state IR features of **4-ClO$_4$** versus **3-ClO$_4$**; rate constant data for the amide methanolysis of **3-ClO$_4$**; CIF data for **4-NO$_3$**; complete reference 35; atomic coordinates for all reactants, transition states, intermediates and products. This material is available free of charge via the Internet at http://pubs.acs.org.

■ AUTHOR INFORMATION

Corresponding Author

*E-mail: lisa.berreau@usu.edu. Phone: (435) 797-3509. Fax: (435) 797-3390.

Notes

The authors declare no competing financial interest.

■ ACKNOWLEDGMENTS

We thank the Utah State University Office of Research and Graduate Studies for a SURCO grant (to E.S.E.) as well as the Utah State University Department of Chemistry and Biochemistry for financial support. R.P. thanks the U.S. National Science Foundation (CHE-1152846) for funding.

REFERENCES

(1) *CDC, Morbidity and Mortality Weekly Report*; Center for Disease Control and Prevention: Atlanta, GA, 2005; pp 513−516.
(2) Claudio, E. S.; Godwin, H. A.; Magyar, J. S. *Prog. Inorg. Chem.* **2003**, *51*, 1−144.
(3) Bridgewater, B. M.; Parkin, G. *J. Am. Chem. Soc.* **2000**, *122*, 7140−7141.
(4) Magyar, J. S.; Weng, T.-C.; Stern, C. M.; Dye, D. F.; Rous, B. W.; Payne, J. C.; Bridgewater, B. M.; Mijovilovich, A.; Parkin, G.; Zaleski, J. M.; Penner-Hahn, J. E.; Godwin, H. A. *J. Am. Chem. Soc.* **2005**, *127*, 9495−9505.
(5) Andersen, R. J.; diTargiani, R. C.; Hancock, R. D.; Stern, C. L.; Goldberg, D. P.; Godwin, H. A. *Inorg. Chem.* **2006**, *45*, 6574−6576.
(6) Farrer, B. T.; Pecoraro, V. L. *Curr. Opin. Drug Discovery Dev.* **2002**, *5*, 937−943.
(7) Matzapetakis, M.; Ghosh, D.; Weng, T. C.; Penner-Hahn, J. E.; Pecoraro, V. L. *J. Biol. Inorg. Chem.* **2006**, *11*, 876−890.
(8) Neupane, K. P.; Pecoraro, V. L. *Angew. Chem., Int. Ed.* **2010**, *49*, 8177−8180.
(9) Neupane, K. P.; Pecoraro, V. L. *J. Inorg. Biochem.* **2011**, *105*, 1030−1034.
(10) Chakraborty, S.; Kravitz, J. Y.; Thulstrup, P. W.; Hemminsen, L.; DeGrado, W. F.; Pecoraro, V. L. *Angew. Chem., Int. Ed.* **2011**, *50*, 2049−2053.
(11) Zampella, G.; Neupane, K. P.; De Gioia, L.; Pecoraro, V. L. *Chem.—Eur. J.* **2012**, *18*, 2040−2050.
(12) Zitka, O.; Kukacka, J.; Krizkova, S.; Huska, D.; Adam, V.; Masarik, M.; Prusa, R.; Kizek, R. *Curr. Med. Chem.* **2010**, *17*, 3751−3768.
(13) Gantt, S. L.; Gattis, S. G.; Fierke, C. A. *Biochemistry* **2006**, *45*, 6170−6178.
(14) Dowling, D. P.; Gattis, S. G.; Fierke, C. A.; Christianson, D. W. *Biochemistry* **2010**, *49*, 5048−5056.
(15) Kita, Y.; Nishii, Y.; Higuchi, T.; Mashima, K. *Angew. Chem., Int. Ed.* **2012**, *51*, 5723−5726.
(16) Yashiro, M.; Kawakami, Y.; Taya, J.; Arai, S.; Fujii, Y. *Chem. Commun.* **2009**, 1544−1546.
(17) Yashiro, M.; Sonobe, Y.; Yamamura, A.; Takarada, T.; Komiyama, M.; Fujii, Y. *Org. Biomol. Chem.* **2003**, *1*, 629−632.
(18) Groves, J. T.; Chambers, R. R. *J. Am. Chem. Soc.* **1984**, *106*, 630−638.
(19) Szajna, E.; Makowska-Grzyska, M. M.; Wasden, C. C.; Arif, A. M.; Berreau, L. M. *Inorg. Chem.* **2005**, *44*, 7595−7605.
(20) Berreau, L. M. *Adv. Phys. Org. Chem.* **2006**, *41*, 79−181.
(21) Berreau, L. M.; Makowska-Grzyska, M. M.; Arif, A. M. *Inorg. Chem.* **2000**, *39*, 4390−4391.
(22) Ingle, G. K.; Makowska-Grzyska, M. M.; Szajna-Fuller, E.; Sen, I.; Price, J. C.; Arif, A. M.; Berreau, L. M. *Inorg. Chem.* **2007**, *46*, 1471−1480.
(23) Szajna-Fuller, E.; Ingle, G. K.; Watkins, R. W.; Arif, A. M.; Berreau, L. M. *Inorg. Chem.* **2007**, *46*, 2353−2355.
(24) Battistuzzi, G.; Borsari, M.; Menabue, L.; Saladini, M.; Sola, M. *Inorg. Chem.* **1996**, *35*, 4239−4247.
(25) Claudio, E. S.; ter Horst, M. A.; Forde, C. E.; Stern, C. L.; Zart, M. K.; Godwin, H. A. *Inorg. Chem.* **2000**, *39*, 1391−1397.
(26) Clapp, L. A.; Siddons, C. J.; Whitehead, J. R.; VanDerveer, D. G.; Rogers, R. D.; Griffin, S. T.; Jones, S. B.; Hancock, R. D. *Inorg. Chem.* **2005**, *44*, 8495−8502.
(27) Bora, R. P.; Ozbil, M.; Prabhakar, R. *J. Biol. Inorg. Chem.* **2010**, *15*, 485−495.
(28) Kumar, A.; Zhu, X.; Walsh, K.; Prabhakar, R. *Inorg. Chem.* **2010**, *49*, 38−46.
(29) Grubel, K.; Fuller, A. L.; Chambers, B. M.; Arif, A. M.; Berreau, L. M. *Inorg. Chem.* **2010**, *49*, 1071−1081.
(30) Allred, R. A.; McAlexander, L. H.; Arif, A. M.; Berreau, L. M. *Inorg. Chem.* **2002**, *41*, 6790−6801.
(31) Wolsey, W. C. *J. Chem. Educ.* **1973**, *50*, A335−A337.
(32) Wilkins, R. G., *Kinetics and Mechanism of Reactions of Transition Metal Complexes*, 2nd ed.; VCH Publishers: New York, 1991.
(33) Altomare, A.; Burla, M. C.; Camalli, M.; Cascarano, G. L.; Giacovazzo, C.; Guagliardi, A.; Moliterni, A. G. G.; Polidori, G.; Spagna, R. *J. Appl. Crystallogr.* **1999**, *32*, 115−119.
(34) Sheldrick, G. M. *SHELXL-97*; University of Göttingen: Göttingen, Germany, 1997.
(35) Frisch, M. J., et al. *Gaussian 09*; Gaussian, Inc.: Wallingford, CT, 2009.
(36) Hay, P. J.; Wadt, W. R. *J. Chem. Phys.* **1985**, *82*, 270−283.
(37) Becke, A. D. *Phys. Rev. A* **1988**, *38*, 3098−3100.
(38) Becke, A. D. *J. Chem. Phys.* **1993**, *98*, 5648−5652.
(39) Shimoni-Livny, L.; Glusker, J. P.; Bock, C. W. *Inorg. Chem.* **1998**, *37*, 1853−1867.
(40) Pellissier, A.; Bretonnière, Y.; Chatterton, N.; Pècaut, J.; Delangle, P.; Mazzanti, M. *Inorg. Chem.* **2007**, *46*, 3714−3725.
(41) Williams, N. J.; Gan, W.; Reibenspies, J. H.; Hancock, R. D. *Inorg. Chem.* **2009**, *48*, 1407−1415.
(42) Zhang, Z.; Xinahe, B.; Zhu, Z.; Chen, R. *Chin. J. Inorg. Chem.* **1997**, *13*, 58.
(43) Farina, P.; Latter, T.; Levason, W.; Reid, G. *Dalton Trans.* **2013**, *42*, 4714−4724.
(44) Park, I.-H.; Park, K.-M.; Lee, S. S. *Dalton Trans.* **2010**, *39*, 9696−9704.
(45) Kuppers, H.-J.; Weighardt, K.; Nuber, B.; Weiss, J. *Z. Anorg. Allg. Chem.* **1989**, *577*, 155−164.
(46) Makowska-Grzyska, M. M.; Doyle, K.; Allred, R. A.; Arif, A. M.; Bebout, D. C.; Berreau, L. M. *Eur. J. Inorg. Chem.* **2005**, 822−827.
(47) Shannon, R. D. *Acta Crystallogr.* **1976**, *A32*, 751−767.
(48) Parkin, G. *Adv. Inorg. Chem.* **1995**, *42*, 291−393.
(49) Nakamoto, K. *Infrared and Raman Spectra of Inorganic and Coordination Compounds*, 5th ed.; John Wiley & Sons, Inc.: New York, 1997; Vol. Part B.
(50) Lipscomb, W. N.; Sträter, N. *Chem. Rev.* **1996**, *96*, 2375−2434.
(51) Brown, R. S.; Hingerty, B. E.; Dewan, J. C.; Klug, A. *Nature* **1983**, *303*, 543−546.
(52) Brown, R. S.; Dewan, J. C.; Klug, A. *Biochemistry* **1985**, *24*, 4785−4801.
(53) Kuusela, S.; Lonnberg, H. *J. Phys. Org. Chem.* **1992**, *5*, 803−811.
(54) Pearson, R. G. *J. Am. Chem. Soc.* **1963**, *85*, 3533−3539.
(55) Raycroft, M. A.; Maxwell, C. I.; Oldham, R. A.; Andrea, A. S.; Neverov, A. A.; Brown, R. S. *Inorg. Chem.* **2012**, *51*, 10325−10333.
(56) Maxwell, E.; Neverov, A. A.; Brown, R. S. *Org. Biomol. Chem.* **2005**, *3*, 4329−4336.
(57) Sayre, L. M. *J. Am. Chem. Soc.* **1986**, *108*, 1632−1635.
(58) Hegg, E. L.; Burstyn, J. N. *Coord. Chem. Rev.* **1998**, *173*, 133−165.
(59) Harrowfield, J. *Helv. Chim. Acta* **2005**, *88*, 2430−2433.